



Susceptible-infected-susceptible model of disease extinction on heterogeneous directed population networks

Elad Korngut ^{1,*} Jason Hindes,² and Michael Assaf ^{1,†}

¹*Racah Institute of Physics, Hebrew University of Jerusalem, Jerusalem 91904, Israel*

²*U.S. Naval Research Laboratory, Code 6792, Plasma Physics Division, Washington, DC 20375, USA*



(Received 18 August 2022; accepted 9 November 2022; published 5 December 2022)

Understanding the spread of diseases through complex networks is of great interest where realistic, heterogeneous contact patterns play a crucial role in the spread. Most works have focused on mean-field behavior—quantifying how contact patterns affect the emergence and stability of (meta)stable endemic states in networks. On the other hand, much less is known about longer time scale dynamics, such as disease extinction, whereby inherent process stochasticity and contact heterogeneity interact to produce large fluctuations that result in the spontaneous clearance of infection. Here we show that heterogeneity in both susceptibility and infectiousness (incoming and outgoing degree, respectively) has a nontrivial effect on extinction in directed contact networks, both speeding up and slowing down extinction rates depending on the relative proportion of such edges in a network, and on whether the heterogeneities in the incoming and outgoing degrees are correlated or anticorrelated. In particular, we show that weak anticorrelated heterogeneity can increase the disease stability, whereas strong heterogeneity gives rise to markedly different results for correlated and anticorrelated heterogeneous networks. All analytical results are corroborated through various numerical schemes including network Monte Carlo simulations.

DOI: [10.1103/PhysRevE.106.064303](https://doi.org/10.1103/PhysRevE.106.064303)

I. INTRODUCTION

Understanding the dynamics of infectious processes is important both for public health and for basic science [1,2]. For the former, epidemic models can provide control strategies for minimizing disease spread within populations [3,4]. For the latter, general insight can be gained on, e.g., contagion dynamics, which can be applied to other areas from election dynamics to the spread of computer viruses [5,6]. A common approach for modeling epidemic dynamics is to partition a population into different compartments and describe the contagious processes using flux terms between various compartments.

A wide range of compartmental models have been studied in the literature [1], all of which are designed to capture a particular aspect of disease dynamics. In this work, we are interested in endemic dynamics, where infection lingers within a population, past the point of an initial outbreak [7,8]. The simplest model for endemic disease dynamics is described by the susceptible-infected-susceptible (SIS) model [2,4], where the population is divided into susceptible (S) and infected (I) individuals; an infected individual that interacts with a susceptible has a chance to transmit the disease, making the susceptible infected; conversely the infected individual can recover and become susceptible once again, according to some prescribed probability.

At the deterministic (mean-field) level, the SIS model has two equilibrium points: an endemic (stable) state and an absorbing (unstable) extinct state [3]. Due to demographic noise emanating from the discreteness of individuals and stochasticity of the reactions, it is possible that a large fluctuation will bring the system from the stable endemic state to the absorbing extinct state [4,7,9,10]. This noise-driven rare event is only one manifestation of the so-called noise-driven escape, which also includes switching between metastable states (see, e.g., Refs. [11,12]), stochastic fade-out [13], and unusually small or large (extreme) outbreaks [14].

In most cases, such rare events in population dynamics models are considered within a well-mixed or homogeneous setting, where individuals interact with an equal number of neighbors with uniform transition rates. Here, analytical treatment is possible using standard techniques [8,10] or, for higher-dimensional systems, by exploiting time-scale separation [15] or various conservation laws [14]. However, it is known that in heterogeneous networks, in which nodes have varying incoming and outgoing degrees or transition rates, the emergence of an endemic state can be dramatically affected [3,16,17]. This is evident in world trade, health care, and social networks, where heterogeneity in the network connectivity was shown to strongly influence disease spread [18–20].

Rigorously dealing with rare events in heterogeneous networks is highly challenging. Recently, progress has been made in analyzing rare events in networks close to bifurcation, where the dimensionality is reduced [3]. In other works, disease extinction in the realm of the SIS model was studied on simplified network topologies [21], or on small networks using exact calculations [22]. More recently, the

*elad.korngut@mail.huji.ac.il

†michael.assaf@mail.huji.ac.il

mean time to extinction (MTE) was analytically studied on directed networks with partial heterogeneity, either in the incoming or outgoing degree [17,23]. In these works it was also suggested that, in the context of extinction in the SIS model, topologically *homogeneous* networks with *heterogeneous* transition rates (susceptibility and infectiousness) are equivalent to topologically *heterogeneous* directed networks with *homogeneous* transition rates. Furthermore, in Ref. [16] the MTE in the SIS model was studied on undirected degree-heterogeneous networks with weak degree dispersion, within an annealed network approximation. Here, the authors showed that the degree dispersion suffices to determine the MTE in the leading order. Yet, rigorously dealing with the full extent of heterogeneity, both in the incoming and outgoing degree, and computing the MTE in this case, has not been carried out in the literature so far.

In this work we extend the formalism developed in Refs. [16,17] and use a semiclassical approach to compute the MTE in the SIS model, for fully heterogeneous, directed networks with arbitrary dispersion. We show that correlation between the population network's incoming and outgoing degrees can greatly affect the MTE: correlation in the degrees brings about a decrease in the MTE, while weak anticorrelation can dramatically increase the MTE. We also compute perturbatively the effect of strong heterogeneity, and show that here, too, correlation and anticorrelation in the incoming and outgoing degrees give rise to markedly different behaviors.

Our paper is organized as follows. In Sec. II we introduce a model employing a topologically homogeneous network with heterogeneous transition rates, and establish its equivalence to degree-heterogeneous networks with homogeneous rates, under the annealed network approximation. We then analyze homogeneous networks with bimodal transition rates and explore such networks numerically in Sec. III, and analytically in Sec. IV, for both weak and strong heterogeneity. Finally, in Sec. V we conclude our results and discuss possible generalizations.

II. THEORETICAL FORMULATION

A. Model

We begin by formulating the SIS model on a topologically homogeneous network with heterogeneous transition rates. Following the notation of Refs. [17,24], we assume an isolated population of N individuals that is divided into k groups, with group i ($i = 1, 2, \dots, k$) consisting of N_i individuals. We denote $f_i = N_i/N$ the proportion of the population in group i , where $\sum_i f_i = 1$. Each group is comprised of susceptible individuals, S , and infected individuals, I . The tendency of an infected individual from group i to infect its neighbors is referred to as its infectiousness, λ_i , whereas susceptibility, μ_i , measures the tendency of an individual from group i to become infected due to an infected neighbor. Thus, the individual's infection and recovery rates of group i are

$$I_i \xrightarrow{W_+(I_i)} I_i + 1, \quad I_i \xrightarrow{W_-(I_i)} I_i - 1, \quad (1)$$

where $W_+(I_i) = (\beta/N)(\sum_{j=1}^k \lambda_j I_j) \mu_i (N_i - I_i)$ is the infection rate, which depends on the susceptibility of group i and the collective infectiousness, while $W_-(I_i) = \gamma I_i$ is the

recovery rate. In addition, β and γ are overall measures of infectiousness and recovery rates, N is the number of nodes (individuals) in the network, and I_i is the number of infected individuals in group i [17,24].

Without loss of generality we can scale λ_i and μ_i such that the average infectiousness $\langle \lambda \rangle$ and average susceptibility $\langle \mu \rangle$ satisfy $\langle \lambda \rangle = \sum_i \lambda_i f_i = 1$ and $\langle \mu \rangle = \sum_i \mu_i f_i = 1$. Defining the fraction of infected in group i by $y_i = I_i/N$, using rates (1), and ignoring demographic fluctuations, the corresponding mean-field rate equations for the average fractions of infected read

$$\dot{y}_i = \beta \left(\sum_{j=1}^k \lambda_j y_j \right) \mu_i (f_i - y_i) - \gamma y_i. \quad (2)$$

Equation (2) has an unstable extinction state, $y_i = 0$, and a stable endemic state, y_i^* , which depends on the transition rates. Notably, the endemic state exists when the basic reproduction number, R_0 , defined by [17,25,26]

$$R_0 = (\beta/\gamma) \sum_{i=1}^k \lambda_i \mu_i f_i, \quad (3)$$

is greater than 1.

Yet, demographic noise and the fact that the extinct state is absorbing renders the stable fixed point metastable [4,7]. Accounting for such noise, the master equation for $P(\mathbf{I}, t)$, the probability to find at time t infected groups $\mathbf{I} = \{I_1, \dots, I_k\}$, reads

$$\frac{\partial P(\mathbf{I}, t)}{\partial t} = \sum_{j=1}^k [W_-(I_j + 1)P(\mathbf{I} + \mathbf{1}_j, t) - W_-(I_j)P(\mathbf{I}, t) + W_+(I_j - 1)P(\mathbf{I} - \mathbf{1}_j, t) - W_+(I_j)P(\mathbf{I}, t)], \quad (4)$$

where an increase and decrease by one of group I_j is denoted by $\mathbf{I} \rightarrow \mathbf{I} \pm \mathbf{1}_j$ [9]. Solving this master equation is, in general, analytically impossible, due to the high dimensionality and complex coupling between the degrees of freedom. Below, we show how to treat this master equation for a homogeneous network with bimodal rates (or bimodal degree distributions). Notably, a generalization to arbitrary symmetric networks, and also weakly asymmetric networks (with small skewness), is possible, using a similar derivation that appears in Ref. [16].

The above formalism holds for well-mixed populations, where the contagion process is assumed to occur between groups with different transition rates. We now show that the latter is equivalent to networks with heterogeneous topology of the incoming and outgoing degrees, under the annealed network approximation, for which the topology is assumed to vary much faster than the transition rates. This results in a contagion process which is established on an average network, where connections are formed according to degree-dependent probability distributions [2]. In such topologically heterogeneous networks nodes are categorized into groups, where each group i has a well-defined incoming degree $d_{\text{in}}(i)$ and outgoing degree $d_{\text{out}}(i)$, resulting in $k < N$ different groups of nodes. Here, we can denote ν as the rate at which infection transmits along each edge and by $k_0^{(\text{in})}$ and $k_0^{(\text{out})}$ the average incoming and outgoing degrees such that $k_0^{(\text{in})} = k_0^{(\text{out})} \equiv k_0$ (with no excess edges). As a result, the infection rate of a

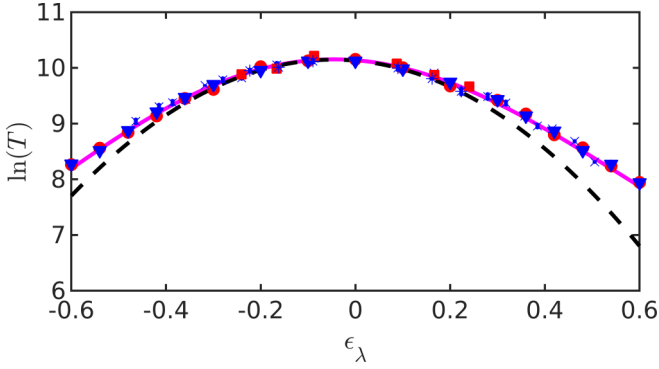


FIG. 1. The logarithm of the MTE versus ϵ_λ for $N = 300$, $R_0 = 1.3$, $k_0 = 100$, and $\epsilon_\mu = 0.1$. Symbols are MC simulations; for each point the MTE and error bar are computed by averaging over 10 networks and 100 realizations per network, according to the scheme presented in Sec. III. Results are shown for networks with bimodal (circle) and Gaussian (square) rate distributions, and bimodal (triangle), Gaussian (asterisk), and gamma (x) degree distributions. Here and henceforth, the size of the error bars is limited by the symbol sizes. The solid line is the numerical solution of Eq. (4) for bimodal networks, while the dashed line is the solution to Eq. (14) (see Sec. IV).

susceptible node i satisfies

$$\frac{\nu}{Nk_0} \left(\sum_{j=1}^k d_{\text{out}}(j) I_j \right) d_{\text{in}}(i) (N_i - I_i), \quad (5)$$

which coincides with $W_+(I_i)$ in Eq. (1) upon choosing $\beta = \nu k_0$, $\mu_i = d_{\text{in}}(i)/k_0$, and $\lambda_i = d_{\text{out}}(i)/k_0$ [17].

B. The case of bimodal networks

We now use a toy model of heterogeneity in the form of bimodal networks. We first numerically corroborate the equivalence between heterogeneity in degree and heterogeneity in rates (for bimodal as well as other networks), and then rigorously study master equation (4) and the MTE for bimodal susceptibility and infectiousness.

Our starting point is a homogeneous network with heterogeneous rates. Here, for bimodal rates there are two well-mixed interacting populations $I_{1,2}$ with infectiousness $\lambda_{1,2}$, susceptibility $\mu_{1,2}$, and transition rates given by Eq. (1), with $k = 2$. We now define $\epsilon_\mu, \epsilon_\lambda \in [-1, 1]$ as the coefficients of variation (CVs) of the infectiousness and susceptibility, respectively, which equal the distributions' standard deviation divided by its mean. In the bimodal case, using the CVs the rates can be rewritten as $\lambda_1 = 1 - \epsilon_\lambda$, $\lambda_2 = 1 + \epsilon_\lambda$, $\mu_1 = 1 - \epsilon_\mu$, and $\mu_2 = 1 + \epsilon_\mu$. Comparing Eqs. (1) and (5), one immediately obtains an equivalence with a network of bimodal incoming and outgoing degree distributions with CVs, $\epsilon_{\text{in}}, \epsilon_{\text{out}} \in [-1, 1]$, upon choosing $\epsilon_\mu = \epsilon_{\text{in}}$ and $\epsilon_\lambda = \epsilon_{\text{out}}$. This can be seen in Fig. 1, where we compare the predictions of the master equation for the MTE with Monte Carlo (MC) simulations, and show the equivalence between degree and rate heterogeneity, for bimodal and other types of networks. The numerical scheme used to obtain Fig. 1 is presented in Sec. III. Note that this figure demonstrates that the MTE is equivalent

for networks with different degree (or rate) distributions, as long as their CV is kept fixed.

Notably, in all our comparisons between different networks and different sources of heterogeneity, we keep the distance from the threshold R_0 constant, thereby ensuring that the stability of the disease-free (extinct) state remains the same. Using Eq. (3), keeping a constant R_0 requires adjusting the ratio β/γ for varying susceptibilities and infectiousness; for bimodal networks, this implies maintaining the equality $\beta/\gamma = R_0/(1 + \epsilon_\lambda \epsilon_\mu)$.

We now analyze the stochastic dynamics and find the MTE in the bimodal case. Here, rate equations (2) for the two infected populations, $y_1(t)$ and $y_2(t)$, satisfy

$$\frac{dy_i}{dt} = \frac{R_0}{1 + \epsilon_\lambda \epsilon_\mu} (\lambda_1 y_1 + \lambda_2 y_2) \mu_i \left(\frac{1}{2} - y_i \right) - y_i, \quad (6)$$

where $i = 1, 2$. To account for stochasticity, we use master equation (4) with $k=2$. Notably, even in this simple case an exact solution to the master equation cannot be found in general. Yet, one can use accurate approximation schemes such as the Wentzel-Kramers-Brillouin (WKB) method [9] to study large deviations and the MTE. The WKB method utilizes a small parameter (in our case $1/N \ll 1$) in order to approximately solve the master equation in a singular limit (see below). Notably, as we will show, the results greatly simplify when heterogeneity is either weak or strong.

To study large deviation in such systems, we assume that after a short time transient the system enters into a long-lived metastable endemic state, and stays there for very long times, on the order of the MTE. This means that stochasticity causes the metastable probability distribution to slowly “leak” into the absorbing state. Thus we write $P(\mathbf{I}) = \mathbf{Q}(\mathbf{I})e^{-t/T}$ where T is the MTE and $\mathbf{Q}(\mathbf{I})$ is the quasistationary distribution (QSD)—the shape of the metastable state. Here the metastable state slowly decays in time at a rate $1/T$, while simultaneously the extinction probability grows and reaches the value of 1 at $t \rightarrow \infty$ [7,9]. We now assume that $N \gg 1$, plug the metastable ansatz into the master equation [Eq. (4)], and employ the WKB approximation for the QSD, $\mathbf{Q}(\mathbf{I}) \equiv \mathbf{Q}(\mathbf{y}) \sim e^{-N\mathcal{S}(\mathbf{y})}$. This results in a stationary Hamilton-Jacobi equation $H(\mathbf{y}, \partial_{\mathbf{y}}\mathcal{S}) = 0$ [9], where $\mathcal{S}(\mathbf{y})$ is the action, and the Hamiltonian satisfies

$$H = \frac{\beta}{\gamma} \left(\sum_{j=1}^k \lambda_j y_j \right) \sum_{i=1}^k \mu_i (f_i - y_i) (e^{p_i} - 1) + \sum_{i=1}^k y_i (e^{-p_i} - 1), \quad (7)$$

with $p_i = \partial_{y_i} \mathcal{S}$ being the momentum of group i , and $k = 2$ for the bimodal case [27]. As a result, the Hamilton's equations, $\dot{y}_i = \partial_{p_i} H$ and $\dot{p}_i = -\partial_{y_i} H$, read

$$\begin{aligned} \dot{y}_i &= \frac{\beta}{\gamma} \left(\sum_{j=1}^k \lambda_j y_j \right) \mu_i (f_i - y_i) e^{p_i} - y_i e^{-p_i}, \\ \dot{p}_i &= -\frac{\beta}{\gamma} \lambda_i \sum_{j=1}^k \mu_j (f_j - y_j) (e^{p_j} - 1) \\ &\quad + \frac{\beta}{\gamma} \left(\sum_{j=1}^k \lambda_j y_j \right) \mu_i (e^{p_i} - 1) - (e^{-p_i} - 1). \end{aligned} \quad (8)$$

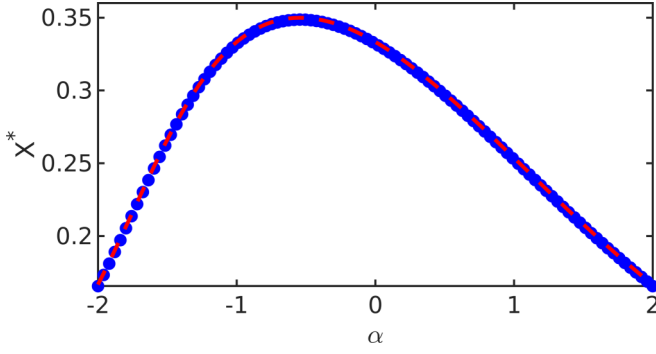


FIG. 2. The mean population fraction of infected individuals in the endemic state, X^* , in the bimodal case, as a function of the CV ratio, $\alpha = \epsilon_\mu/\epsilon_\lambda$, for $N = 2000$, $R_0 = 1.5$, and $\epsilon_\lambda = 0.5$. Symbols are numerical solutions to the master equation, while the dashed curve is given by Eqs. (9).

The fixed points in the extended phase space ($\{y_i\}, \{p_i\}$) can be found, for any degree or rate distribution, by equating Eqs. (8) to zero [17,28]. In the bimodal case, $i = 1, 2$, we find

$$y_i^* = \frac{\mu_i D(\epsilon_\lambda, \epsilon_\mu)}{2[1 + \mu_i D(\epsilon_\lambda, \epsilon_\mu)]}, \quad p_i^* = -\ln[1 + \lambda_i D'], \quad (9)$$

where $D(\epsilon_\lambda, \epsilon_\mu) = \zeta + [\zeta^2 + (R_0 - 1)/(1 - \epsilon_\mu^2)]^{1/2}$, D' is identical to $D(\epsilon_\lambda, \epsilon_\mu)$ upon replacing ϵ_λ and ϵ_μ , and $\zeta = R_0/[2(1 + \epsilon_\lambda \epsilon_\mu)] - 1/(1 - \epsilon_\mu^2)$. Denoting $X^* = y_1^* + y_2^*$ as the population fraction of the total number of infected in the endemic state, Eq. (9) with $\epsilon_\lambda = \epsilon_\mu = 0$, agrees with the known homogeneous fixed point, $X^* = x_0 \equiv (R_0 - 1)/R_0$. However, for populations where both the susceptibility and infectiousness are heterogeneous, the endemic population can be greater than x_0 as can be seen in Fig. 2. Indeed, denoting the CVs ratio by $\alpha = \epsilon_\mu/\epsilon_\lambda$, for $\alpha > 0$ the population's infectiousness and susceptibility are correlated, while for $\alpha < 0$ they are anticorrelated. Notably, the maximum of X^* is obtained for anticorrelated rates, which will have a strong impact on the MTE in this regime (see below).

C. Mean time to extinction

In order to find the MTE, one has to find the action function, $\mathcal{S}(\mathbf{y})$, by solving Hamilton's equations (8) either numerically or analytically. Below we show how these equations can be solved numerically (Sec. III) and analytically (Sec. IV). Having found the action function, the MTE in the leading order satisfies [7]

$$T \sim e^{N\Delta\mathcal{S}}, \quad \Delta\mathcal{S} = \int_0^\infty \mathbf{p}\dot{\mathbf{y}}dt = \mathcal{S}(\mathbf{0}) - \mathcal{S}(\mathbf{y}^*), \quad (10)$$

where $\Delta\mathcal{S}$ is the action barrier along the optimal path to extinction [9] and \mathbf{y}^* is the endemic fixed point.

So far, Eq. (10) has been computed analytically in three special cases. For homogeneous rates, $\epsilon_\lambda = \epsilon_\mu = 0$, one has $\Delta\mathcal{S}_0 = \ln R_0 + 1/R_0 - 1$ [4,7]. In the case of partial

heterogeneity in the susceptibility, using real space [7] and momentum space [42] calculations, one finds [17]

$$\begin{aligned} \Delta\mathcal{S}(0, \epsilon_\mu) &= \frac{1}{2} \ln[1 + (1 - \epsilon_\mu)D(0, \epsilon_\mu)] \\ &+ \frac{1}{2} \ln[1 + (1 + \epsilon_\mu)D(0, \epsilon_\mu)] - \frac{D(0, \epsilon_\mu)}{R_0}, \end{aligned} \quad (11)$$

where $D(\epsilon_\lambda, \epsilon_\mu)$ is defined below Eq. (9), and a similar result holds for partial heterogeneity in the infectiousness. Finally, in the case of undirected networks, $\epsilon_\lambda = \epsilon_\mu = \epsilon$, a general result has been found in the case of $\epsilon \ll 1$ [16]:

$$\begin{aligned} \Delta\mathcal{S}(\epsilon) &= S_0 - h(R_0)\epsilon^2, \\ h(R_0) &= \frac{(R_0 - 1)(1 - 12R_0 + 3R_0^2) + 8R_0^2 \ln(R_0)}{4R_0^3}. \end{aligned} \quad (12)$$

Below we generalize these results and solve the Hamilton's equations with heterogeneity present in both rates.

III. NUMERICAL SIMULATIONS

To corroborate our analytical findings, and to study directed heterogeneous networks in parameter regimes that are inaccessible to analytical treatment, we used three numerical methods to compute the MTE [29]. Below, we present these methods from the most accurate but slowest, to the least accurate but fastest.

The first method included performing kinetic MC simulations on directed heterogeneous networks. Here, we generated a network satisfying the annealed network approximation and employed Gillespie's algorithm to mimic the SIS dynamics [30–32]. For each node in a network there is an exponentially distributed time to make a transition to another state. When the rates are heterogeneous and the topology is homogeneous, each node has a different rate of susceptibility and infectiousness but the same number of neighbors. On the other hand, when the degree distribution is heterogeneous, each node has a different incoming and outgoing degree but the same transition rates, and the annealed network approximation is used. For correlated networks, degrees (or rates) were paired with the same ranking (the highest outgoing degree coupled with the highest incoming degree) in contrast with anticorrelated networks, where degrees (or rates) were paired with opposite ranking (highest outgoing degree coupled with lowest incoming degree or vice versa). To account for the variability across different networks, we generated several different network realizations, computed the MTE on each network realization, and then averaged over all networks. For each particular network, the simulated extinction times were fitted to an exponential distribution, where the resulting mean and confidence bounds were treated as the MTE and its confidence bounds of the network. The mean over all networks yielded the overall MTE, whereas the standard deviation of the confidence bounds provided the MTE's error bars. Out of the three methods, this method was the most time consuming with runtime that grows exponentially with increasing reproductive number and population size; yet it mimics the stochastic dynamics in the most accurate way, and it is applicable to any generic degree or rate distribution.

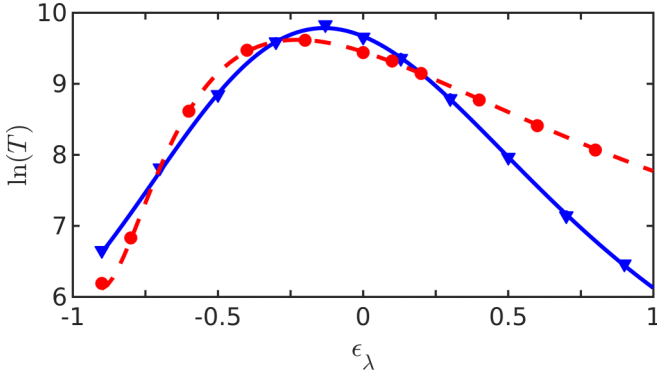


FIG. 3. The logarithm of the MTE versus ϵ_λ . Lines are solutions of the master equation, while symbols are MC simulations; for each point the MTE is computed by averaging over 100 stochastic realizations for a fully connected network with a given rate distribution, and then averaging over 10 different network realizations with the same rate distribution. The errors were found to be smaller than the symbol size. Parameters are $N = 400$, $R_0 = 1.25$, $\epsilon_\mu = 0.3$ (triangles); $N = 200$, $R_0 = 1.5$, and $\epsilon_\mu = 0.8$ (circles). The maximum MTE was obtained at $\epsilon_\lambda = -0.13$ and $\epsilon_\lambda = -0.25$, for networks with $\epsilon_\mu = 0.3$ and $\epsilon_\mu = 0.8$, respectively.

The second method included a numerical solution of the master equation, by finding the largest eigenvalue of the matrix in Eq. (4), the inverse of which is the MTE, whereas the corresponding eigenvector represents the QSD [33]. This method was only used for the bimodal case ($k = 2$); here each population has anywhere between zero and $N/2$ infected individuals, and thus the matrix dimensionality in Eq. (4) is $(N/2 + 1)^2$ for $k = 2$. As shown in Figs. 1 and 3, this method provides highly accurate results for the MTE, including preexponential corrections, unlike the solution to the Hamilton's equations (see below). Furthermore, this method is highly advantageous in terms of running time compared to the MC simulations, as long as $k \leq 2$. For $k > 2$, however, this method becomes less feasible when N is large, as one has to deal with a matrix of $\mathcal{O}(N^k)$ dimensions, and thus the runtime grows exponentially with increasing k .

To demonstrate that the master equation description, which effectively assumes the annealed network approximation [2], can be used to accurately compute the MTE [33], we compare in Fig. 3 its predictions with MC simulations (see also Fig. 1). We do so for bimodal networks, and plot the MTE as a function of ϵ_λ for two distinct values of ϵ_μ . Here, the prediction of the master equation for the MTE excellently agrees with that of MC simulations, as long as the average number of neighbors of each node is large [34]. One can clearly see in Fig. 3 the asymmetry of the curves with respect to the transition point between correlated and anticorrelated degree distributions (i.e., $\epsilon_\lambda = 0$). Importantly, the maximal MTE is not obtained in the homogeneous scenario, but rather when the infectiousness and susceptibility are anticorrelated (see Sec. IV A).

The third method we used included solving the Hamilton's equations [Eqs. (8)] numerically. To do so, we used the iterative action minimization method [3,35,36], which allows finding the path $\mathbf{p}(\mathbf{y})$ along the heteroclinic (or zero-energy) trajectory, connecting the endemic fixed point $(\mathbf{y}, \mathbf{p}) = (\mathbf{y}^*, \mathbf{0})$

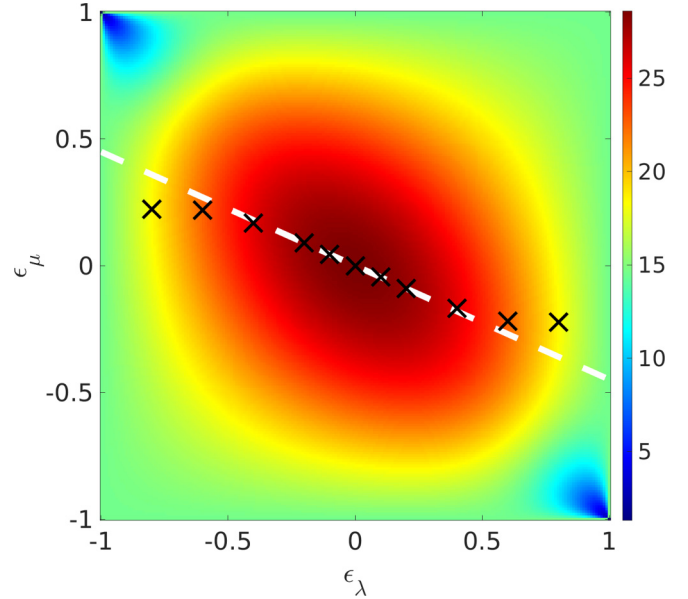


FIG. 4. A heatmap of the logarithm of the MTE, $\ln(T)$, obtained by solving the master equation in the bimodal case versus ϵ_λ and ϵ_μ . Here $N = 400$ and $R_0 = 1.5$. The x's mark the value of ϵ_μ which maximizes the MTE for a given ϵ_λ , while the dashed line denotes the theoretical prediction for this maximum (see Sec. IV A), formally valid for weak heterogeneity.

with the extinction state $(\mathbf{y}, \mathbf{p}) = (\mathbf{0}, \mathbf{p}^*)$ [17]. Once $\mathbf{y}(t)$ and $\mathbf{p}(t)$ are found along the optimal path, we use Eq. (10) to calculate the action. Notably, unlike the MC simulations and numerical solution of the master equation, this method provides the MTE up to exponential accuracy and misses the preexponential factor. Yet, it is highly advantageous timewise, as it includes finding solutions to only $2k$ ordinary differential equations for each time step along the zero-energy path. Typically, a quasi-Newtonian method can be used to solve the equations, with quadratic time complexity in the number of time steps and k . Thus, while we have focused on the bimodal case, this method can be used to deal with any degree (or rate) distribution, with arbitrary k (see details in Ref. [3]).

Figure 4 shows numerical solutions of the master equation for the entire phase space in the bimodal case. We notice that the figure is symmetrical to reflection along either horizontal or vertical axis. This is due to the duality property, which states that for any generic network with SIS dynamics denoted by \mathbf{T} , where T_{ij} indicates the rate at which individual j infects individual i , the action barrier remains unchanged under the transposition of matrix \mathbf{T} . For our model, $T_{ij} = \beta \lambda_j \mu_i / N$, which suggests that the action remains the same under the exchange of μ and λ and that $\Delta\mathcal{S}(\epsilon_\lambda, \epsilon_\mu) = \Delta\mathcal{S}(\epsilon_\mu, \epsilon_\lambda)$ [17,37–39]. The rest of the paper will be devoted to finding analytical expressions for $\Delta\mathcal{S}(\epsilon_\lambda, \epsilon_\mu)$ in two main regions: weak heterogeneity and strong heterogeneity.

IV. RESULTS

We now use perturbation theory to analyze two important parameter regions: weak and strong heterogeneity.

A. Weak heterogeneity

Here we analyze the case of weak heterogeneity, where $\epsilon_\lambda, \epsilon_\mu \ll 1$. In this limit we can Taylor-expand $\Delta S(\epsilon_\lambda, \epsilon_\mu)$, the action barrier to extinction, up to second order:

$$\begin{aligned} \Delta S(\epsilon_\lambda, \epsilon_\mu) &\simeq \Delta S(0, 0) + \left(\frac{\partial \Delta S}{\partial \epsilon_\lambda}\right) \epsilon_\lambda + \left(\frac{\partial \Delta S}{\partial \epsilon_\mu}\right) \epsilon_\mu \\ &+ \frac{1}{2} \left(\frac{\partial^2 \Delta S}{\partial \epsilon_\lambda^2}\right) \epsilon_\lambda^2 + \left(\frac{\partial^2 \Delta S}{\partial \epsilon_\lambda \partial \epsilon_\mu}\right) \epsilon_\lambda \epsilon_\mu \\ &+ \frac{1}{2} \left(\frac{\partial^2 \Delta S}{\partial \epsilon_\mu^2}\right) \epsilon_\mu^2, \end{aligned} \quad (13)$$

where all derivatives are evaluated at $\epsilon_\lambda = \epsilon_\mu = 0$. Next, we will show that these terms can be evaluated using Eq. (11), Ref. [16], and the duality property.

First, the leading-order term satisfies $\Delta S(0, 0) = \Delta S_0 = \ln R_0 + 1/R_0 - 1$, since $\epsilon_\lambda = \epsilon_\mu = 0$ and the problem is reduced to one dimension [4,7].

To evaluate the first-order terms with respect to ϵ_λ or ϵ_μ , we notice that Eq. (11) provides the action when only one of the rates includes heterogeneity. For example, to find $\partial_{\epsilon_\mu} \Delta S$ at $\epsilon_\lambda = \epsilon_\mu = 0$, we can differentiate Eq. (11) with respect to ϵ_μ and substitute $\epsilon_\mu = 0$, which yields $\partial_{\epsilon_\mu} \Delta S(0, \epsilon_\mu) = 0$. The same result is obtained for $\partial_{\epsilon_\lambda} \Delta S$ at $\epsilon_\lambda = \epsilon_\mu = 0$, as $S(0, \epsilon) = S(\epsilon, 0)$ (duality principle). Therefore, both first-order terms vanish in Eq. (13).

We now proceed to computing the second-order terms in Eq. (13), where there are three such terms. The derivatives $\partial_{\epsilon_\mu}^2 \Delta S$ and $\partial_{\epsilon_\lambda}^2 \Delta S$ can be computed at $\epsilon_\lambda = \epsilon_\mu = 0$ in the same way as the first-order terms, using Eq. (11). This yields $\partial_{\epsilon_\lambda}^2 \Delta S = \partial_{\epsilon_\mu}^2 \Delta S = -x_0^2$ [40]. To compute the mixed derivative in Eq. (13), we define $\psi(R_0)$ such that $\psi(R_0)x_0^2/2 = -\partial_{\epsilon_\lambda} \partial_{\epsilon_\mu} \Delta S$, evaluated at $\epsilon_\lambda = \epsilon_\mu = 0$. As a result, the action barrier becomes

$$\Delta S(\epsilon_\lambda, \epsilon_\mu) \simeq \Delta S_0 - \frac{x_0^2}{2} \epsilon_\lambda^2 [1 + \psi(R_0)\alpha + \alpha^2], \quad (14)$$

where, to remind the reader, $\alpha = \epsilon_\mu/\epsilon_\lambda$. To find $\psi(R_0)$, we compare Eq. (14) with Eq. (12) in the case of undirected networks. Putting $\alpha = 1$, we find $\psi(R_0) = 2[h(R_0) - x_0^2]/x_0^2$, where $h(R_0)$ is given by Eq. (12).

Equation (14) is our first main result. It generalizes the results of Refs. [16,17] to directed heterogeneous networks, and predicts up to subleading-order corrections the MTE, which only depends on the CVs of both rates, and the reproductive number. A comparison between our analytical solution for the MTE, using Eqs. (10) and (14) and a numerical solution of the Hamilton's equations, can be seen in Fig. 5, and excellent agreement is observed. Importantly, although our derivation has been carried out for bimodal networks, Eq. (14) holds for generic networks of arbitrary degree (or rate) distributions, with CVs, ϵ_μ and ϵ_λ , of the incoming (susceptibility) and outgoing (infectiousness) degrees, respectively. This is demonstrated in Fig. 1 for various networks, with bimodal, Gaussian, and gamma distributions.

How does $\psi(R_0)$ behave with R_0 ? Close to the bifurcation, at $R_0 - 1 \ll 1$, it can be shown that in the leading order, $h(R_0) \simeq 3/2(R_0 - 1)^2 \simeq 3/2x_0^2$. As a result, at $R_0 - 1 \ll 1$, $\psi(R_0) \simeq 1$. As R_0 increases, the value of $\psi(R_0)$ decreases

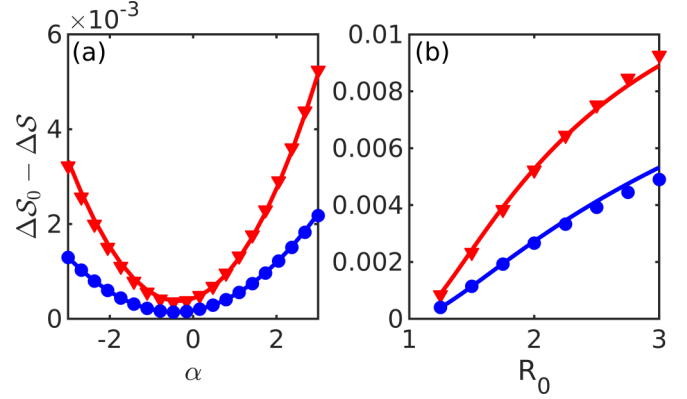


FIG. 5. The correction to the action for weak heterogeneity. (a) $\Delta S_0 - \Delta S$ versus α . Symbols are solutions to the Hamilton's equations for $\epsilon_\lambda = 0.05$, with $R_0 = 1.6$ (circles) and $R_0 = 2.4$ (triangles). Solid curves are the theoretical predictions [Eq. (14)]. (b) $\Delta S_0 - \Delta S$ versus R_0 . Symbols are solutions to the Hamilton's equations for $\epsilon_\lambda = 0.08$, with $\alpha = 0.5$ (triangles) and $\alpha = -0.5$ (circles). Solid curves are the theoretical predictions [Eq. (14)].

monotonically. Thus, since $\psi(R_0) \leq 1$ for any R_0 , the action barrier in the presence of heterogeneous rates is always smaller than that in the fully homogeneous case. However, given heterogeneity in, say, only the incoming degrees, with homogeneous outgoing degree, the MTE can be *increased* by adding heterogeneity in the outgoing degree as well. This result is counterintuitive, as in most cases adding heterogeneity increases overall fluctuations, which decrease the stability of the metastable state and, thus, decrease the MTE.

Indeed, having found the dependence of the action barrier on α for weakly heterogeneous networks, we can find the value of α for which the MTE is maximized. Doing so, we find $\alpha_{\max} = -\psi(R_0)/2$, or $\epsilon_\mu = -[\psi(R_0)/2]\epsilon_\lambda$ [41]. For R_0 close to 1, the maximum is obtained at $\alpha = -1/2$, and as R_0 increases, the maximum decreases in its absolute value. This behavior can be seen in Figs. 4 and 6. Notably, the maximum of the MTE is obtained at a negative value of α , namely, when the heterogeneity in the incoming degree is anticorrelated with that of the outgoing degree. This is evident also by looking at Fig. 6(b). On the one hand, the mean fraction of total infected is maximized at $\alpha = -1/2$ regardless of the value of R_0 , which is the dominant factor for the fact that the MTE is maximized at this value of α or close to it. On the other hand, the minimum of the relative width of the QSD (or relative fluctuations), obtained at $\alpha \simeq -1/2$ for $R_0 - 1 \ll 1$, shifts towards zero as R_0 increases. These two effects cause the maximum of the MTE to also shift from $\alpha = -1/2$ towards $\alpha = 0$ as R_0 is increased. This also indicates that anticorrelation between the incoming and outgoing degrees decreases (for any R_0) the typical fluctuations, which brings about an increase in the disease stability and MTE (see Figs. 4–6).

B. Strong heterogeneity

Here we analyze the case of strong heterogeneity in either the infectiousness or susceptibility. We denote by $\delta = 1 - \epsilon$ the distance from maximal heterogeneity, and assume δ is small. Without loss of generality we study the case of strong

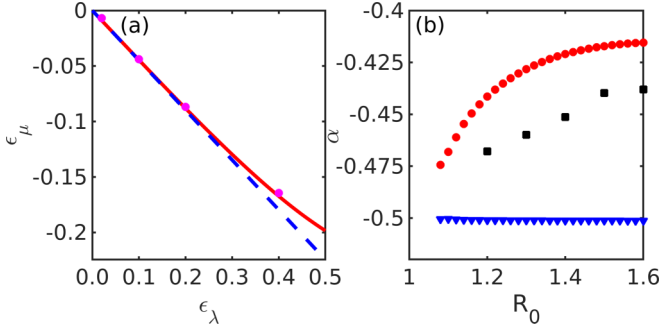


FIG. 6. (a) The value of ϵ_μ for which the MTE is maximized versus ϵ_λ . The solid line shows the numerical solution of the master equation, the circles are numerical solutions of the Hamilton's equations, while the dashed line shows Eq. (14), valid at $\epsilon_\lambda \ll 1$. Parameters are $N = 300$ and $R_0 = 1.5$. (b) The values of α at which (i) X^* receives its maximum (triangles), (ii) the QSD's relative width receives its minimum (circles), and (iii) $\Delta\mathcal{S}$ receives its maximum (squares), versus R_0 . The mean and relative width were obtained by numerically solving the master equation with $N = 2000$, while the action was obtained by solving the Hamilton's equations.

heterogeneity in infectiousness, $\delta_\lambda = 1 - \epsilon_\lambda \ll 1$. Our aim is to compute $\Delta\mathcal{S}$, given by

$$\Delta\mathcal{S} = \int_{y_1^*}^0 p_1(y_1) dy_1 + \int_{y_2^*}^0 p_2(y_2) dy_2. \quad (15)$$

In the correlated case, $\alpha > 0$, it can be shown that the leading $\mathcal{O}(\delta_\lambda^0)$ order of Hamiltonian (7) satisfies

$$H = y_2[e^{-p_2} - 1 + (e^{p_2} - 1)(2y_2 - 1)R_0] + \mathcal{O}(\delta_\lambda). \quad (16)$$

Here, we have assumed that $p_1 \sim \mathcal{O}(\delta_\lambda)$ (see below). Putting $H = 0$ we find that $p_2^{(0)}(y_2) = -\ln[R_0(1 - 2y_2)]$. Integrating over the momentum $p_2(y_2)$ along the extinction path [see Eq. (15)] yields $\Delta\mathcal{S} = \Delta\mathcal{S}_0/2$. This is the action obtained for a well-mixed population of size $N/2$, since half of the population has zero infectiousness, and thus only half of the population participates in the dynamics.

To obtain the δ_λ -dependent correction to this result, we compute the fixed points of the Hamilton's equations [Eqs. (8)], given by Eq. (9), for $\delta_\lambda \ll 1$, which read

$$\begin{aligned} p_1^* &= -\frac{1}{2}(R_0 - 1)\delta_\lambda, \\ p_2^* &= -\ln(R_0) - \frac{(R_0 - 1)(1 - \epsilon_\mu)}{2(1 + \epsilon_\mu)}\delta_\lambda, \\ y_1^* &= \frac{x_0 R_0 (1 - \epsilon_\mu)}{2\xi} \left[1 - \frac{R_0 (1 - \epsilon_\mu) \epsilon_\mu}{\xi^2} \delta_\lambda \right], \\ y_2^* &= \frac{x_0}{2} \left[1 + \frac{(1 - \epsilon_\mu) \epsilon_\mu}{(1 + \epsilon_\mu) \xi} \delta_\lambda \right], \end{aligned} \quad (17)$$

where $\xi = R_0 - (R_0 - 2)\epsilon_\mu$. We now proceed in the same spirit as Ref. [16], and assume the following scaling for the momenta, valid for $\alpha > 0$: $p_1(y_1) = p_1^*(y_1^* - y_1)/y_1^*$ [which scales as $\mathcal{O}(\delta_\lambda)$], and $p_2(y_2) = p_2^{(0)}[y_2(1 + \theta\delta_\lambda)] + [p_2^* + \ln(R_0)](y_2^* - y_2)/y_2^*$, where $p_2^{(0)}$ is given below Eq. (16). In this way, it is guaranteed that $p_1(0) = p_1^*$ and $p_1(y_1^*) = 0$. In addition, $p_2(0) = p_2^*$, as $p_2^{(0)}(0) = -\ln(R_0)$, and the

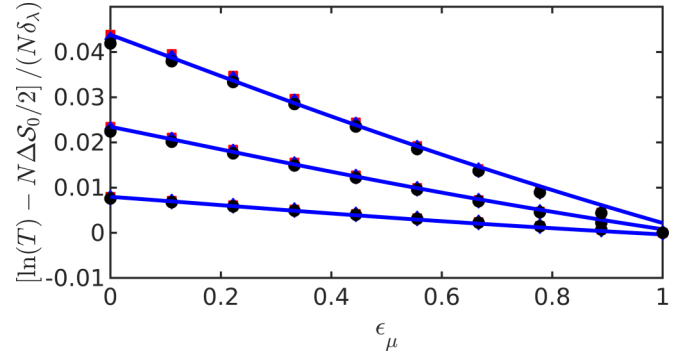


FIG. 7. Shown is the correction to the action, $[\ln(T) - N\Delta\mathcal{S}_0/2]/(N\delta_\lambda)$ as a function of ϵ_μ for $N = 700$. Symbols are numerical solutions to the master equation for $R_0 = 1.2, 1.35, \text{ and } 1.5$ (bottom to top), and for each R_0 , $\delta_\lambda = 0.05, 0.1, \text{ and } 0.15$. Lines are the theoretical prediction (18).

free parameter θ is chosen such that $p_2(y_2^*) = \mathcal{O}(\delta_\lambda^2)$, which yields $\theta = (1 - \epsilon_\mu)\epsilon_\mu/[\xi(1 + \epsilon_\mu)]$. Using these momenta, and keeping terms up to $\mathcal{O}(\delta_\lambda)$, Eq. (15) yields

$$\begin{aligned} \Delta\mathcal{S} &= \frac{\Delta\mathcal{S}_0}{2} + \delta_\lambda \frac{1 - \epsilon_\mu}{4R_0(1 + \epsilon_\mu)\xi} \\ &\quad \times [(R_0 - 1)^2 R_0 + (3 - 4R_0 + R_0^2 + 2R_0 \ln R_0)\epsilon_\mu], \end{aligned} \quad (18)$$

where the δ_λ -dependent correction is positive for $\epsilon_\mu > 0$. Note that the case where susceptibility is large and correlated, resulting in small $\delta_\mu = 1 - \epsilon_\mu \ll 1$, can be treated using the duality property. In Fig. 7 we show that the analytical formula (18) excellently agrees with a numerical solution of the master equation for various values of R_0 and δ_λ . Similarly as for weak heterogeneity, Eq. (18) also holds for generic networks with CVs, ϵ_μ and ϵ_λ , of the incoming and outgoing distributions, respectively.

The case of strong anticorrelation, where one of the ϵ 's is close to 1 and the other is arbitrary and negative, such that $\alpha < 0$, is more intricate. Here, the above method is invalid and the solution can only be found numerically.

An interesting example is the case of extreme anticorrelation, with $\epsilon_\lambda = 1 - \delta = -\epsilon_\mu$ and $\delta \ll 1$. In this case, in the leading order of $\delta \ll 1$, deterministic rate equations (6) yields an unstable extinct state, $y_1^* = y_2^* = 0$, and a stable endemic state $y_1^* = (R_0 - 2)/(2R_0)$ and $y_2^* = 1/2$. This endemic state ceases to exist when $R_0 \leq 2$, where only the extinct state exists and becomes stable. That is, bifurcation in this extreme anticorrelation case occurs at $R_0 = 2$. This is because the first infected group y_1 has almost zero infectiousness but high susceptibility, while the second infected group y_2 has almost zero susceptibility but high infectiousness. Thus, dynamically, the second group is almost autonomous in the leading order, and becomes established (i.e., reaches an endemic fixed point y_2^*) only when the rescaled reproduction number R_0 exceeds 2. Once this occurs, the first infected group can also be established at y_1^* . Only for $R_0 \rightarrow \infty$ the groups become equivalent.

The MTE in the case of extreme anticorrelation can be numerically computed. In Fig. 4 this regime can be seen in the top left and bottom right corners when the MTE is minimal;

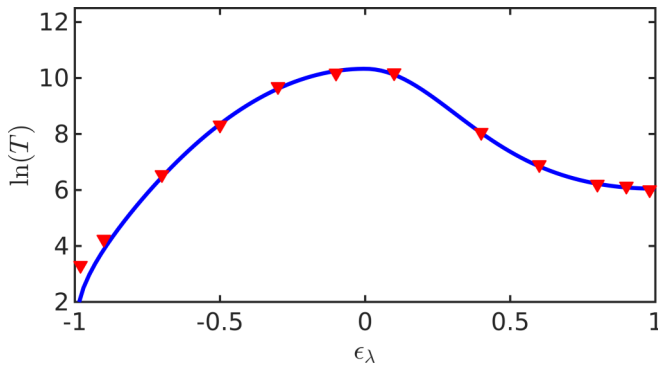


FIG. 8. The logarithm of the MTE, $\ln(T)$, versus ϵ_λ where $\epsilon_\mu = |\epsilon_\lambda|$. The solid line is the solution to the master equation for $N = 300$ and $R_0 = 1.3$, while symbols are MC simulations obtained for a fully connected network with bimodal rates averaged over 10 networks and 100 iterations (see Sec. III).

here for $R_0 < 2$, the endemic state ceases to exist as $\epsilon_\lambda = -\epsilon_\mu \rightarrow 1$ (or vice versa). This can also be observed in Fig. 8, where we choose the same CV magnitude for both rates, but with a different sign. In this figure the extreme anticorrelation case can be seen on the left side where the MTE goes to zero (as the endemic fixed point ceases to exist), whereas extreme correlation can be seen on the right side, where the action approximately converges to half of its maximal value [see Eq. (18)].

V. DISCUSSION

Most studies of disease spread through complex networks focused on short time scales related to the emergence of the endemic state and its relaxation dynamics. On the other hand, the study of longer time scales, relevant for disease extinction, was impeded by the complex topology of these networks. Here we have generalized several recent studies, and investigated, in the realm of the SIS model, disease extinction on heterogeneous and directed population networks. To do so we have used various numerical methods with varying efficiency and accuracy, as well as a semiclassical WKB approximation

to the master equation. The latter provides, in the leading order in the population size, an alternative Hamiltonian formulation of the problem, which can be dealt with rigorously in various parameter regimes.

We initially showed that under the annealed network approximation, heterogeneity in the network topology, i.e. in the individual's incoming and outgoing degrees, is equivalent to heterogeneity in its susceptibility and infectiousness. In particular, the mean time to extinction (MTE) was shown to be identical for degree and rate heterogeneity, by employing Monte Carlo simulations, as well as numerically solving the master equation and the corresponding Hamilton's equations. The numerical schemes were then used to corroborate our analytical findings, mainly in two regimes: weak and strong heterogeneity. While our analytical derivation was carried out on a toy model of bimodal networks with dichotomous heterogeneity, it can be generalized to networks with arbitrary (weakly skewed) incoming and outgoing degree distributions [16]. Importantly, we have shown that correlation or anticorrelation between an individual's incoming (susceptibility) and outgoing (infectiousness) degrees has a dramatic impact on the disease lifetime. It was shown that, for strong heterogeneity, anticorrelation tends to always decrease the MTE. On the other hand, for weak heterogeneity, anticorrelation between the incoming and outgoing degrees can increase disease stability and the MTE, which is counterintuitive, as in most cases heterogeneity tends to decrease stability.

Although it is beyond the scope of this paper, it would be interesting to explore how asymmetry in the degree (or rate) distribution, which appears, e.g., in strongly skewed distributions such as those with power-law tails, affects the mean time to disease clearance and its statistics.

ACKNOWLEDGMENTS

E.K. and M.A. acknowledge support from the ISF Grant No. 531/20. M.A. also acknowledges the Alexander von Humboldt Foundation for an experienced researcher fellowship.

-
- [1] H. W. Hethcote, The mathematics of infectious diseases, *SIAM Rev.* **42**, 599 (2000).
 - [2] R. Pastor-Satorras, C. Castellano, P. Van Mieghem, and A. Vespignani, Epidemic processes in complex networks, *Rev. Mod. Phys.* **87**, 925 (2015).
 - [3] J. Hinde and I. B. Schwartz, Epidemic Extinction and Control in Heterogeneous Networks, *Phys. Rev. Lett.* **117**, 028302 (2016).
 - [4] I. Nåsell, *Extinction and Quasi-stationarity in the Stochastic Logistic SIS Model* (Springer, Berlin, 2011).
 - [5] A. Volkening, D. F. Linder, M. A. Porter, and G. A. Rempala, Forecasting elections using compartmental models of infection, *SIAM Rev.* **62**, 837 (2020).
 - [6] L. Billings, W. Spears, and I. Schwartz, A unified prediction of computer virus spread in connected networks, *Phys. Lett. A: Gen. At. Solid State Phys.* **297**, 261 (2002).
 - [7] M. Assaf and B. Meerson, Extinction of metastable stochastic populations, *Phys. Rev. E* **81**, 021116 (2010).
 - [8] M. Assaf and B. Meerson, WKB theory of large deviations in stochastic populations, *J. Phys. A: Math. Theor.* **50**, 263001 (2017).
 - [9] M. I. Dykman, E. Mori, J. Ross, and P. M. Hunt, Large fluctuations and optimal paths in chemical kinetics, *J. Chem. Phys.* **100**, 5735 (1994).
 - [10] O. Ovaskainen, The quasistationary distribution of the stochastic logistic model, *J. Appl. Probab.* **38**, 898 (2001).
 - [11] M. Assaf, E. Roberts, and Z. Luthey-Schulten, Determining the Stability of Genetic Switches: Explicitly Accounting for mRNA Noise, *Phys. Rev. Lett.* **106**, 248102 (2011).
 - [12] B. Schäfer, M. Matthiae, X. Zhang, M. Rohden, M. Timme, and D. Witthaut, Escape routes, weak links, and desynchronization

- in fluctuation-driven networks, *Phys. Rev. E* **95**, 060203(R) (2017).
- [13] D. Coombs, R. Straube, and M. Ward, Diffusion on a sphere with localized traps: Mean first passage time, eigenvalue asymptotics, and Fekete points, *SIAM J. Appl. Math.* **70**, 302 (2009).
- [14] J. Hindes, M. Assaf, and I. B. Schwartz, Outbreak Size Distribution in Stochastic Epidemic Models, *Phys. Rev. Lett.* **128**, 078301 (2022).
- [15] M. I. Dykman, I. B. Schwartz, and A. S. Landsman, Disease Extinction in the Presence of Random Vaccination, *Phys. Rev. Lett.* **101**, 078101 (2008).
- [16] J. Hindes and M. Assaf, Degree Dispersion Increases the Rate of Rare Events in Population Networks, *Phys. Rev. Lett.* **123**, 068301 (2019).
- [17] D. Clancy, Persistence time of SIS infections in heterogeneous populations and networks, *J. Math. Biol.* **77**, 545 (2018).
- [18] N. C. Banks, D. R. Paini, K. L. Bayliss, and M. Hodda, The role of global trade and transport network topology in the human-mediated dispersal of alien species, *Ecol. Lett.* **18**, 188 (2015).
- [19] K. C. King and C. M. Lively, Does genetic diversity limit disease spread in natural host populations? *Heredity* **109**, 199 (2012).
- [20] G. E. Leventhal, A. L. Hill, M. A. Nowak, and S. Bonhoeffer, Evolution and emergence of infectious diseases in theoretical and real-world networks, *Nat. Commun.* **6**, 6101 (2015).
- [21] F. Fagnani and L. Zino, Time to extinction for the SIS epidemic model: New bounds on the tail probabilities, *IEEE Trans. Network Sci. Eng.* **6**, 74 (2017).
- [22] P. Holme and L. Tupikina, Epidemic extinction in networks: Insights from the 12 110 smallest graphs, *New J. Phys.* **20**, 113042 (2018).
- [23] D. Clancy, Precise estimates of persistence time for SIS infections in heterogeneous populations, *Bull. Math. Biol.* **80**, 2871 (2018).
- [24] D. Clancy and C. Pearce, The effect of population heterogeneities upon spread of infection, *J. Math. Biol.* **67**, 963 (2013).
- [25] O. Diekmann, J. A. P. Heesterbeek, and M. G. Roberts, The construction of next-generation matrices for compartmental epidemic models, *J. R. Soc. Interface* **7**, 873 (2010).
- [26] O. Diekmann, J. Heesterbeek, and J. Metz, On the definition and the computation of the basic reproduction ratio R_0 in models for infectious diseases in heterogeneous populations, *J. Math. Biol.* **28**, 365 (1990).
- [27] In the simple case of $k = 1$, one recovers the Hamiltonian of the usual well-mixed SIS model, $H = R_0 y(1 - y)(e^p - 1) + y(e^{-p} - 1)$, with $\lambda = \mu = 1$, and $R_0 = \beta/\gamma$ [9].
- [28] A. Nold, Heterogeneity in disease-transmission modeling, *Math. Biosci.* **52**, 227 (1980).
- [29] Our codes for the three different numerical simulations were carried out using PYTHON and MATLAB, and are available at <https://github.com/eladkorngut/directed-SIS-simulations>.
- [30] B. K. Fosdick, D. B. Larremore, J. Nishimura, and J. Ugander, Configuring random graph models with fixed degree sequences, *SIAM Rev.* **60**, 315 (2018).
- [31] M. Molloy and B. Reed, A critical point for random graphs with a given degree sequence, *Random Struct. Algorithms* **6**, 161 (1995).
- [32] D. T. Gillespie, Exact stochastic simulation of coupled chemical reactions, *J. Phys. Chem.* **81**, 2340 (1977).
- [33] M. J. Keeling and J. V. Ross, On methods for studying stochastic disease dynamics, *J. R. Soc. Interface* **5**, 171 (2008).
- [34] In this case, the mean-field-like structure of the infection rate in master equation (4) is justified as long as one averages over an ensemble of networks.
- [35] B. S. Lindley and I. B. Schwartz, An iterative action minimizing method for computing optimal paths in stochastic dynamical systems, *Physica D* **255**, 22 (2013).
- [36] M. Bauer, E. Forgoston, and L. Billings, Computing the optimal path in stochastic dynamical systems, *Chaos* **26**, 083101 (2016).
- [37] R. R. Wilkinson and K. J. Sharkey, An exact relationship between invasion probability and endemic prevalence for Markovian SIS dynamics on networks, *PLoS One* **8**, 1 (2013).
- [38] R. A. Holley and T. M. Liggett, Ergodic theorems for weakly interacting infinite systems and the voter model, *Ann. Probab.* **3**, 643 (1975).
- [39] T. E. Harris, On a class of set-valued Markov processes, *Ann. Probab.* **4**, 175 (1976).
- [40] The fact that these derivatives are identical stems from the duality principle, namely, $\Delta\mathcal{S}$ remains unchanged under the exchange of ϵ_μ and ϵ_λ .
- [41] Here, due to the duality principle, we can exchange ϵ_λ and ϵ_μ and leave the action barrier unchanged.
- [42] M. Assaf, B. Meerson, and P. V. Sasorov, Large fluctuations in stochastic population dynamics: momentum-space calculations, *J. Stat. Mech.: Theory Exp.* (2010) P07018.